Preparation of in situ ZIF-9 grown on sodium alginate/polyvinyl alcohol hydrogels for enhancing Cu (II) adsorption from aqueous solutions

Zhang guojun (1036613870@qq.com)
Chen Huiyuan
Yang Guijun
Fu Hua

Research Article

Keywords: Sodium alginate hydrogel, ZIF-9, Cu (II), adsorption

Posted Date: June 8th, 2022

DOI: https://doi.org/10.21203/rs.3.rs-1710832/v1

Preparation of in situ ZIF-9 grown on sodium alginate/polyvinyl alcohol hydrogels for enhancing Cu (II) adsorption from aqueous solutions

Guojun Zhang[a], HuiYuan Chen[a], Guijun Yang[a], Hua Fu[a,*1]

ABSTRACT

Metal-organic framework materials(ZIF-9) were loaded on Sodium alginate/polyvinyl(PVA/SA) hydrogel by in situ growth method for adsorption of heavy metal Cu (II). The structure of hydrogels composited with MOFs and polymers was designed to improve the poor mechanical properties of natural polymer gel materials and the inconvenience of powdered MOFs materials in practical applications. The adsorption results showed that the optimum adsorption process of Cu (II) pH was 5.0. The adsorption kinetics and isotherm suggest that the adsorption process follows the Freundlich isotherm and the pseudo-second-order models. The experimental maximum adsorption capacity was 98.98 mg/g, 2.6 times and 1.5 times higher than ordinary SA and PVA/SA hydrogel spheres. Synthesized hydrogel spheres were characterized by FT-IR, SEM, XRD, and XPS, which confirmed that MOF materials have grown in situ on PVA/SA hydrogel spheres. More importantly, PVA/SA@ZIF-9 exhibited exceptional mechanical stability and showed excellent recycling capability in the cyclic adsorption process.

Keywords:

Sodium alginate hydrogel. ZIF-9. Cu (II). adsorption

[*] Corresponding author. fuhua8711@126.com

[a] College of Chemical Engineering, Qinghai University, Xining, 810016, China

1 Introduction

Water is a significant, meaningful resource for social and economic development. The rapid growth of human activities and industrialization has caused severe heavy metal pollution problems in water. The commonly used treatment methods for heavy metal pollution in water are chemical precipitation[1], electrochemical treatment[2], membrane treatment[3], ion exchange[4], and adsorption methods. Among them, the adsorption method has the advantages of simple operation, low cost, and environmental friendliness, making it become one of the most potential technologies widely used in treating heavy metal pollution in water. [5-8]. A large number of adsorbent materials have already been applied to the treatment of heavy metal pollution in water, such as modified cellulose materials[9], activated carbon fiber material[10], nanocrystalline materials[11], magnetic nanomaterials [12], etc. However, seeking high-efficiency and novel adsorption materials and applying them to the field of heavy metal treatment in water is still a hot research topic for scholars. In recent years, the application of hydrogel adsorbents treating heavy metals in water has received extensive attention. The hydrogel material is a polymer compound that has abundant adsorption active sites on its network polymer chain, such as -OH, $-NH_2$, -COOH, $-SO_3H$, $-CONH_2$, etc., so it can remove the target metal ions from the contaminated water by effectively interacting with the target metal. Based on environmental friendliness and economic cost considerations, natural polymer materials have been widely used in heavy metal pollution treatment in water[13]. Common natural polymers include cellulose, chitosan, sodium alginate, etc. Among them, sodium alginate, as a natural polysaccharide, is rich in carboxyl (-COOH) and hydroxyl (-OH) functional groups. It reacts with multivalent metal ions such as Ca(II) and Fe(III) to form a gel with a three-dimensional network structure, which has the advantage of good solid-liquid separation when used in water[14]. In addition, it has the advantages of good biocompatibility,

biodegradability, comprehensive source, and economic availability. However, applying a single sodium alginate hydrogel material also has shortcomings, such as limited adsorption active sites and poor mechanical properties[15], which limit its practical use due to possible difficulties such as disintegration. It has been reported that biochar[16], cellulose[17], gelatin [18], and other materials are blended and embedded with sodium alginate to enhance their mechanical strength and other properties. Li [19]et al. prepared apatite/attapulgite/alginate composite hydrogels to adsorb aqueous solution methylene blue (MB). It was stated that the apatite and attapulgite particles enhanced the hydrogel structure. At the same time, the composite gel with attapulgite and apatite added increased the porosity and effectively active adsorbed sites, improving the affinity of the hydrogel surface. Compared to conventional alginate hydrogels, it has a higher adsorption capacity.

Metal-organic frameworks (MOFs), as a new type of porous material, usually have the advantages of high porosity, large surface area, and controllable composition. These benefits allow MOFs to be synthesized by various methods and widely studied in wastewater treatment and resource recovery applications[20]. However, most of the current MOFs reported are in powder form. The practical application of powdered MOFs was limited due to the disadvantages of poor processability, recyclability, and potential safety hazards of dust formation. Some processing steps are required to address these issues to improve the machinability of MOFs in practical applications. The easiest way is to bond MOFs particles using a binder to form bulky particles directly. However, this often reduces surface area and severe pore plugging[21]. Another approach is combining MOFs with other materials to create composite materials, which produce synergistic effects that enhance material functionality[22 - 24]. ZIF-9 is a powdered MOFs material prepared with Co^{2+} as a metal ion and benzimidazole (bIm) as an organic ligand. Like most other powdered MOFs, there are certain defects in the

practical application process.

Therefore, the final product combines the advantages of the natural polymer material SA containing significant adsorption functional groups porous structure of MOFs materials, using PVA/SA hydrogels as the matrix, loading ZIF-9 by in situ growth method hydrogels in this study. It solves the problems of poor mechanical properties of SA hydrogels and inconvenient application of MOFs powder materials. Conventional methods characterized the prepared PVA/SA@ZIF-9 composites; total reflection Fourier transform infrared spectroscopy (ATR-FTIR), field emission scanning electron microscopy (FE-SEM), and X-ray electron spectroscopy (XPS), Brunauer-Emmett-Teller(BET), X-ray diffraction. Finally, the prepared PVA/SA@ZIF-9 material was applied to Cu(Ⅱ) adsorption. The adsorption pH, adsorption kinetics, adsorption isotherm, adsorption thermodynamics, and recycling performance during the adsorption process were studied by adsorption experiments, which verified the application potential of the adsorbent.

2 Materials

SA [$(C_6H_7NaO_6)m$], PVA [$(C_2H_4O)n$], calcium chloride ($CaCl_2$), Cobalt Nitrate [$Co(NH_3)_2{\cdot}6H_2O$], Benzimidazole (bIm), N,N'-Dimethylformamide (DMF)were obtained from Macklin Biochemical Co.,Ltd (Shanghai,China). cupric nitrate [$(Cu(NO_3)_2{\cdot}3H_2O)$], hydrochloric acid (HCl), sodium hydroxide (NaOH), and sodium chloride (NaCl) were obtained from Sinopharm Chemical Reagent Co., Ltd (Shanghai, China). A stock Cu(II) solution of 1000 mg/ L was prepared and further diluted to the desired levels for later use.

3 Experiment and methods

3.1 Preparation of PVA/SA gel spheres

2.81 g SA powder was dissolved in 100 mL of PVA (2.48%, w/v) as solution A. After stirring vigorously for 3 h, the PVA/SA solution was dropped into 300 mL $CaCl_2$ solution (2.4%, w/v) with a syringe needle. The PVA/SA

hydrogels obtained were soaked in the $CaCl_2$ solution for 24 hours to ensure complete gelation. The uncross-linked calcium ions on the surface of the hydrogels were washed with distilled water. According to the different contents of sodium alginate SA (2.5, 3.0, 3.5, 4g), the as-prepared PVA/SA composite hydrogels were named PVA/SA-2.5, PVA/SA-3.0, PVA/SA-3.5, PVA/SA-4.0. A part of hydrogels was stored in water for later use. The rest of the hydrogel spheres were freeze-dried.

3.2 Preparation of PVA/SA@ZIF-9 gel spheres

The PVA/SA hydrogels were placed in 100mL 58.7g/L $Co(NO_3)_2 \cdot 6H_2O$ N N'-Dimethylformamide solution and stirred for 12 h. Hydrogels were washed with N'-Dimethylformamide solution three times to remove unabsorbed ions. Then all hydrogels were added to 23.5g/L benzimidazole N N'-Dimethylformamide solution, and 6 ml of ammonia water was slowly added dropwise during stirring. After being stirred for 12 h, hydrogels were washed with N'-Dimethylformamide solution three times to remove unbound benzimidazole. The PVA/SA@ZIF-9 composite hydrogels were dried in a vacuum drying oven at 60℃ and stored to use in Cu(II) adsorption.

3.2 Adsorption experiment

The Cu(II) solution was obtained by diluting 1000 mg/L Cu(II) stock solution $(CuNO_3)_2 \cdot 3H_2O$) by the stepwise dilution method and sealed at 4℃. 0.05g of PVA/SA hydrogel adsorbents were added to 50mL of Cu(II) solution with a concentration of 20-500mg/L and shaken at a constant temperature shaker (160 rpm). The pH of the Cu(II) solution was adjusted between 2 and 6 with 0.1mol HCl/NaOH solution. The effect of adsorption time on the capacity of Cu(II) solution was investigated. The remaining concentration of Cu(II) in the solution after adsorption was confirmed by ICP-OES. The removal rate of Cu(II) by the adsorbent (R, %), the adsorption capacity (q_t, mg/g) corresponding to

any time t (min), and the equilibrium adsorption capacity (q_e, mg/g) were calculated as follows :

$$R(\%) = \frac{c_0 - c_e}{c_0} \times 100 \quad (1)$$

$$q_t = \frac{c_0 - c_t}{m} \times V \quad (2)$$

$$q_e = \frac{c_0 - c_e}{m} \times V \quad (3)$$

where C_0, C_t, C_e represent the Cu(II) concentration (mg/L) in the solution at the initial time, time t, and equilibrium, respectively; m is the dry weight of the adsorbent; V is the Cu(II) solution (L) volume. The experimental adsorption data are the average value of two or more repeated experiments.

3.3 adsorption-desorption experiments

The desorption steps were as follows: The PVA/SA/@ZIF-9-Cu(II) hydrogels were put into 50 mL of 0.2 mol/L HCl with mechanically stirring at 200 rpm at 25℃ for 2 h. Then the hydrogels above were repeatedly washed with deionized water until the pH of the aqueous solution was neutral, and then the regeneration of PVA/SA/@ZIF-9 hydrogels was repeated 8 times for the Cu(II) adsorption.

3.4 Characterization analysis

Fourier transform infrared(FTIR, Nicolet 6700 Thermo fisher, USA) spectroscopy was used to analyze the functional groups of hydrogels and adsorption mechanism at the scanning wavenumber range from 650 to 4000 cm^{-1}, the resolution was 4 cm^{-1}, and the reflection accessory was diamond-ATR. The morphology of the composite hydrogels were investigated by field emission scanning electron microscope treated with gold spraying (SEM, JSM-6610LV, Tokyo, Japan). X-ray diffraction(XRD, D8 FOCUS, Germany) was used to explore the crystalline structure of composite hydrogels with CuK α radiation from 5 ° ~65 ° . The detection voltage was 40Kv, the analysis current was 40mA, and the scanning rate was 3° ~5° /min. A 200 mg

sample was weighed for specific surface area testing to calculate the specific surface area of PVA/SA and PVA/SA@ZIF-9 using the Brunauer-Emmett-Teller(BET) method and N_2 adsorption-desorption isotherms at 77 K to evaluate their pore structure. Vacuum degassing for 6 h at 120 ° C. (Autosorb-iQ2, Quantachroe, USA). The chemical elements were analyzed by X-ray photoelectron spectroscopy (XPS, ESCALAB, Thermo Fisher, USA) spectrometer before and after modification and adsorption. The binding energy was corrected with C ls (284.8 eV). Avantage software processed the resulting spectrum for peak separation.

4 Results and discussion

4.1 Analysis of Preparation Materials

4.1.1 FT-IR Analysis

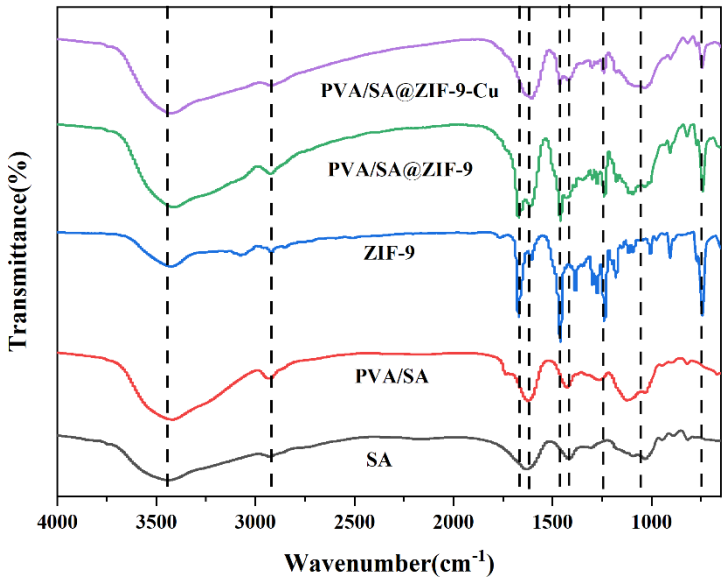

Fig. 1: FTIR spectra of SA, PVA/SA, ZIF-9, PVA/SA/@ZIF-9, and PVA/SA/@ZIF-9-Cu hydrogels

The FTIR spectra of SA, PVA/SA, ZIF-9, PVA/SA/@ZIF-9, and PVA/SA/@ZIF-9-Cu hydrogels were shown in Fig. 1. The wideband at 3600-

3000cm^{-1} corresponded to the stretching vibration of -OH[25]. The peaks at 2800-3000cm^{-1} were attributed to the C-H (-CH or -CH_2) stretching vibration. Since PVA was rich in -OH and C-H groups, the FTIR spectra of PVA/SA, -OH, and C-H stretching vibration are significantly more robust than SA hydrogels. In addition, the peaks of 1620cm^{-1} and 1419cm^{-1} were the asymmetric and symmetric stretching vibrations of carboxylate (-COO-), respectively[26]. The peaks of 1070cm^{-1} were due to the C-OH bond of the alcoholic hydroxyl group[27]. In the FTIR spectra of PVA/SA-ZIF-9, the peaks of 3440cm^{-1} belong to the benzimidazole -NH stretching vibration. The peaks of 1670cm^{-1} were stretching vibration of the benzene ring, the peaks at 1460cm^{-1} and 1240cm^{-1}were -C-H and C-C stretching vibration on benzimidazole, the peaks at 742cm^{-1} were the stretching vibration of the -CH on the benzene ring[28]. ZIF-9 material was successfully grown in situ on the PVA/SA hydrogels from the results above. After the PVA/SA@ZIF-9 hydrogels were combined with Cu(II), -COO-groups belonging to the carboxylate moved to the low frequency (from 1620 to 1600cm^{-1}, 1419 to 1410cm^{-1}); the positions of the characteristic peaks changed obviously, which indicated that the hydrogels material participated various reactions during the possible process of Cu(II) adsorption.

4.1.2 Morphological characteristics of SA, PVA, PVA/SA/@ZIF-9

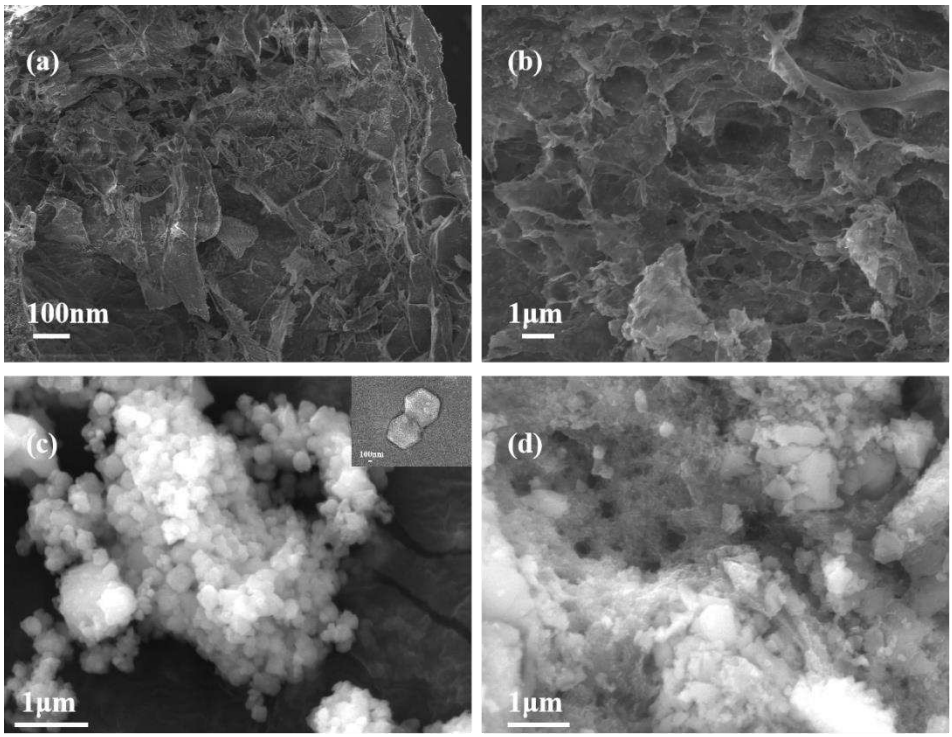

Fig. 2：(a) SA, (b) PVA/SA, (c) ZIF-9, SEM images of pure ZIF-9 in the upper right corner, (d) SEM images of PVA/SA/@ZIF-9

Fig. 2 (a) showed the morphology of SA under the emission scanning electron microscope; the surface of SA was relatively smooth and flat. Fig. 2 (b) showed the morphology of PVA/SA. Comparing with the SA hydrogel, the material after composite PVA has a more apparent lamellar structure, which was conducive to the diffusion of heavy metal ions during the adsorption process of the material and increased the active adsorption sites of the material. Fig. 2 (c) was the SEM image of ZIF-9, the Crystal structure was shown in the upper right corner, the pore structure image of the hydrogel (Fig. 2 d) showed that ZIF-9 crystals are attached and embedded, and its porous structure has not changed due to the loading of ZIF-9.

4.1.3 XRD analysis

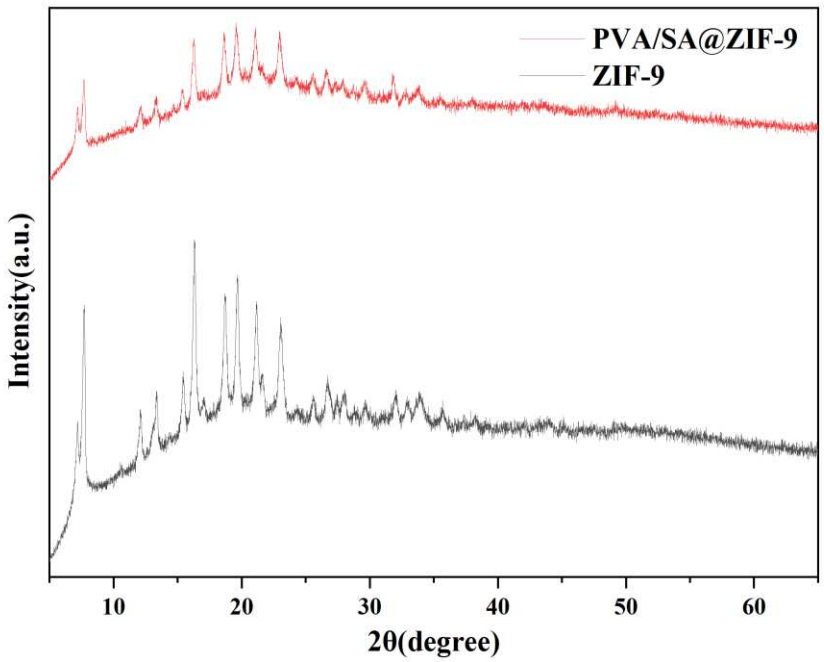

Fig. 3: XRD patterns of ZIF-9, PVA/SA/@ZIF-9

Fig. 3 shows the XRD pattern of the ZIF-9 and PVA/SA/@ZIF-9 composite material, showing that the XRD pattern of the PVA/SA/@ZIF-9 composite was consistent with the ZIF-9 pattern, indicating that the crystal structure of ZIF-9 was supported by PVA/SA hydrogel through in situ growth method was not affected. A few characteristic peaks of ZIF-9 were weakened, probably because ZIF-9 was coated by sodium alginate and polyvinyl alcohol in PVA/SA hydrogel. However, it also shows that PVA/SA/@ZIF-9 composite material preparation was successful.

4.1.4 BET analysis

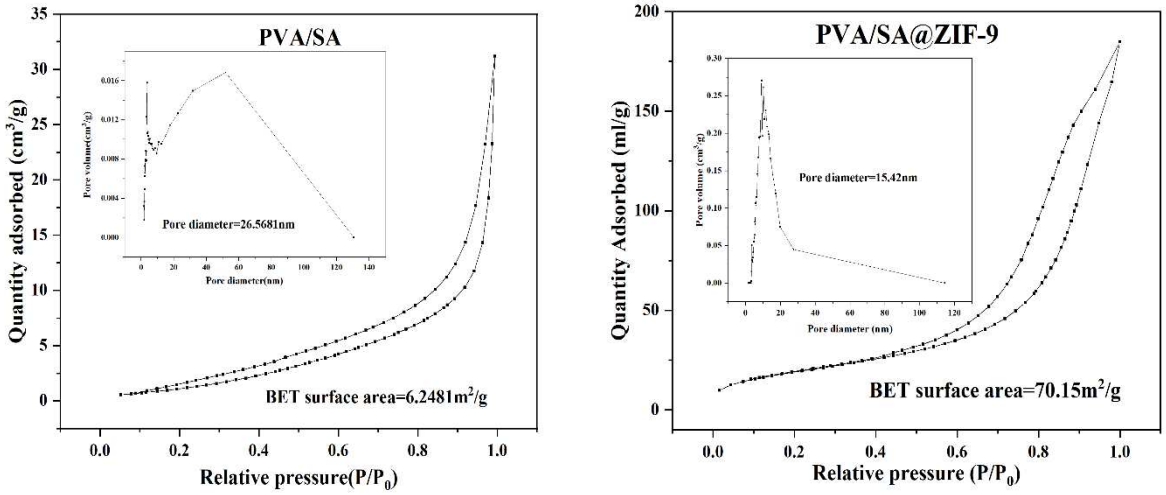

Fig. 4： N_2 adsorption and desorption isotherms of PVA/SA and PVA/SA/@ZIF-9, corresponding pore size distributions

The BET test was used to investigate the effect of the in-situ growth of ZIF-9 on the surface of PVA/SA hydrogels on the material's porous structure. The N_2 adsorption-desorption isotherms and pore size distributions of PVA/SA and PVA/SA/@ZIF-9 hydrogels was shown in Fig. 4. The surface area and average pore diameter of PVA/SA were 6.2481m^2/g and 26.56nm, while the surface area and the average pore diameter of PVA/SA@ZIF-9 were 70.1531m^2/g and 15.43nm, which could be attributed to the high specific surface area of ZIF-9. Compared with PVA/SA hydrogels, PVA/SA/@ZIF-9 exhibited a larger specific surface area, indicting by loading ZIF-9 in situ growth to PVA /SA hydrogels, which significantly increased the specific surface area of the material and were beneficial to the adsorption process.

4.1.5 XPS analysis

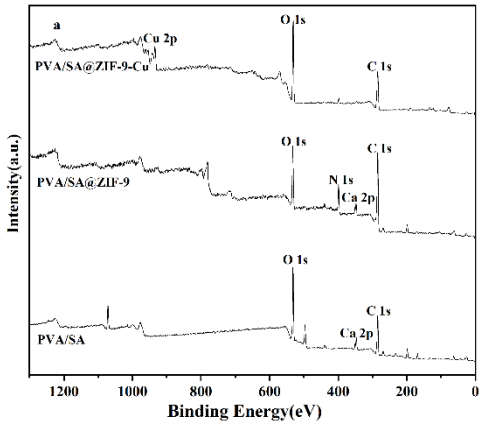

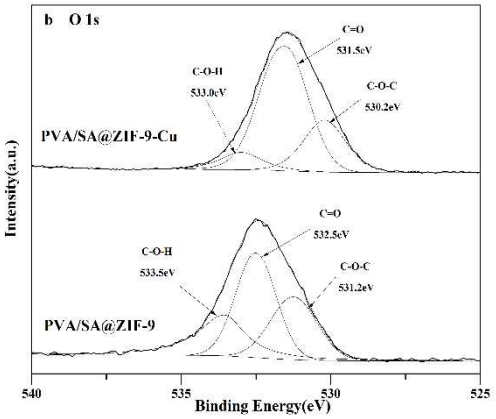

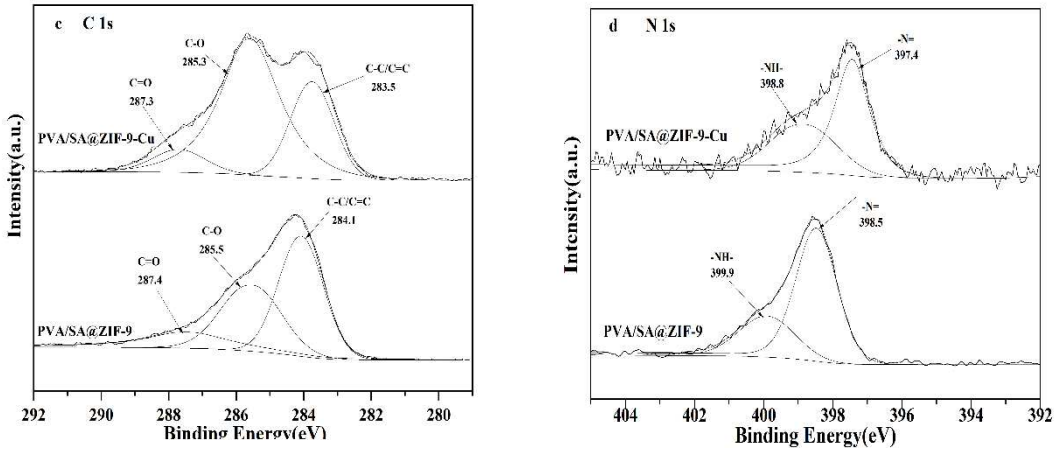

Fig. 5: (a) XPS spectra of PVA/SA, PVA/SA/@ZIF-9, and PVA/SA/@ZIF-9-Cu: wide scan; (b) Spectra of O1s before and after adsorption ; (c) Spectra of C 1s before and after adsorption; (d) Specta of N 1s before and after adsorption.

The element binding energy of PVA/SA, PVA/SA@ZIF-9, and PVA/SA@ZIF-9-Cu were further investigated by using XPS. As shown in Fig. 5 (a), the characteristic peak of N 1s can be observed around 399.5 eV in the PVA/SA/@ZIF-9 hydrogel spectrum. When PVA/SA/@ZIF-9 hydrogel adsorbed Cu(II), a Cu 2p spectrum appeared, indicating that Cu(II) was adsorbed on PVA/SA/@ZIF-9 hydrogel. The characteristic peak of Ca 2p disappears in the PVA/SA/@ZIF-9-Cu hydrogel spectrum, which may be caused by the ion exchange between Cu(II) and Ca(II). The gel morphology of the adsorbent is not destroyed after the adsorption, which proves that the primary interaction with the associated Ca(II) was not completely replaced. In the high-resolution XPS spectrum of O 1s(Fig.6b), it was found that PVA/SA/@ZIF-9 had different peaks of 533.5eV, 532.5eV, and 531.2eV, which were the binding energies by C-OH, C=O, and C-O-C of the composite hydrogel, respectively[29]. While the hydrogel adsorbed Cu(II), its peak value transferred to 533.0eV, 531.5eV, and 530.2eV, respectively. The C 1s spectrum(Fig.6c) shows three peaks, in which 287.4eV and 285.5eV were ascribed to C=O and C-O of the composite hydrogel, and 284.1 eV was the binding energy of C-C[30], respectively. When the material was combined with Cu(II), the binding

energies of C=O, C-O, and C-C transferred to 287.3 eV, 285.3 eV, and 283.5 eV, respectively, indicating that the adsorption process of Cu(II) by composite hydrogel materials involves oxygen-containing functional groups. The peaks of 399.9eV and 399.5eV in the N 1s(Fig.5d) XPS spectrum of PVA/SA/@ZIF-9 hydrogel were the binding energies of -NH- and -N= of benzimidazole in ZIF-9, respectively[31]. After adsorption of Cu(II), the binding energy of N peak transferred to 398.8 eV and 397.4 eV, respectively. The intensity of the N 1s peak was observed to decrease, indicating that ZIF-9 in the composite hydrogel had an adsorption effect on Cu(II).

The FTIR and XPS results suggest that the carboxyl and hydroxyl functional groups had cation exchange and complexing with Cu(II) PVA/SA@ZIF-9 hydrogels and Cu (II) ions, at the same time physical adsorption also played a role. The adsorption mechanism was described in Figure 7.

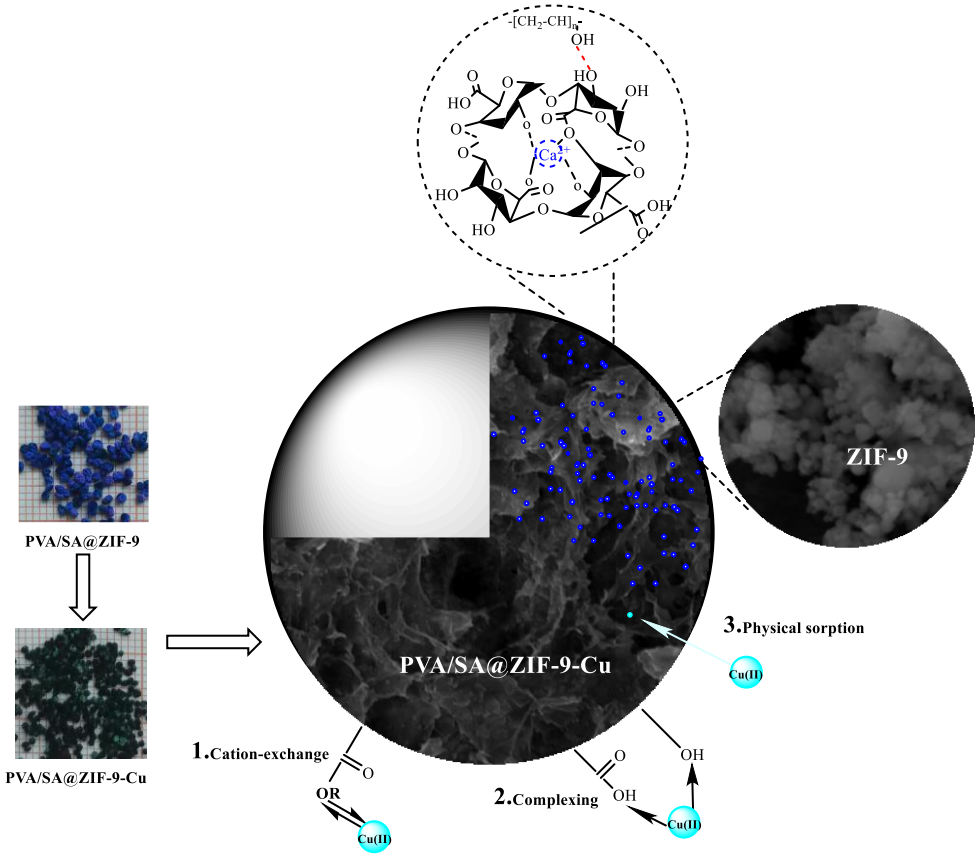

Fig. 6. Adsorption mechanism of PVA/SA@ZIF-9

4.2 Adsorption experimental studies

4.2.1 Effects of pH

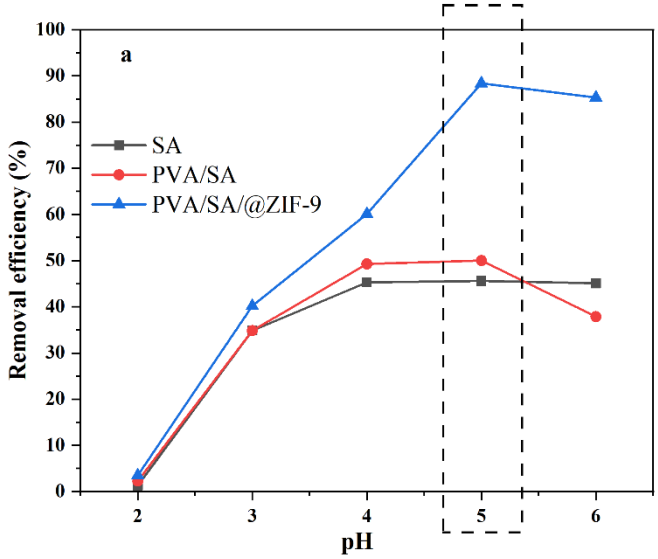

Fig. 7: The effect of pH on the adsorption performance of SA, PVA/SA, PVA/SA@ZIF-9 gel spheres on Cu(II) (Dose=1g/L, C_0=50mg/L, t=24h, T=25℃)

The pH of the aqueous solution directly affects the form of adsorbate in the water and the chemical properties of the adsorbent. Therefore the SA, PVA/SA PVA/SA@ZIF-9 hydrogels were added to the initial Cu(II) concentration of 50mg/L when the pH value of the solution was 2-6. the results were shown in Fig. 7. The three adsorbents have a similar overall change trend under different initial pH values of the solution. As the pH increases from 2 to 6, the removal efficiency of Cu(II) by the three materials increases gradually. PVA/SA and PVA/SA@ZIF-9 reached the maximum removal rate of Cu(II) at pH 5 and then decreased. And PVA/SA@ZIF-9 has a significantly higher removal rate of Cu(II) than the other materials under the research conditions, which may be due to the improved number of adsorption sites and adsorption specific surface area after composite ZIF-9 material. At lower pH, the removal rate is correspondingly lower due to the competitive effect between H^+ and Cu^{2+} for adsorption sites[32]. The competitive relationship weakened

when the pH value gradually increased, the competitive relationship weakened when the pH value gradually increased, and Cu^{2+} had more opportunities to contact the unoccupied adsorption sites, which led to an increase in the removal rate. It was observed in this study that the reduced removal rate of Cu(II) at pH=6 may be due to the formation of partial copper hydroxide precipitation, and functional groups such as -COOH and -OH in the adsorbent cannot interact with this state of Cu(II) binding. In summary, the experimental content of this chapter selects pH 5 as the experimental condition for subsequent adsorption experiments.

4.2.2 Adsorption kinetics and adsorption isotherms

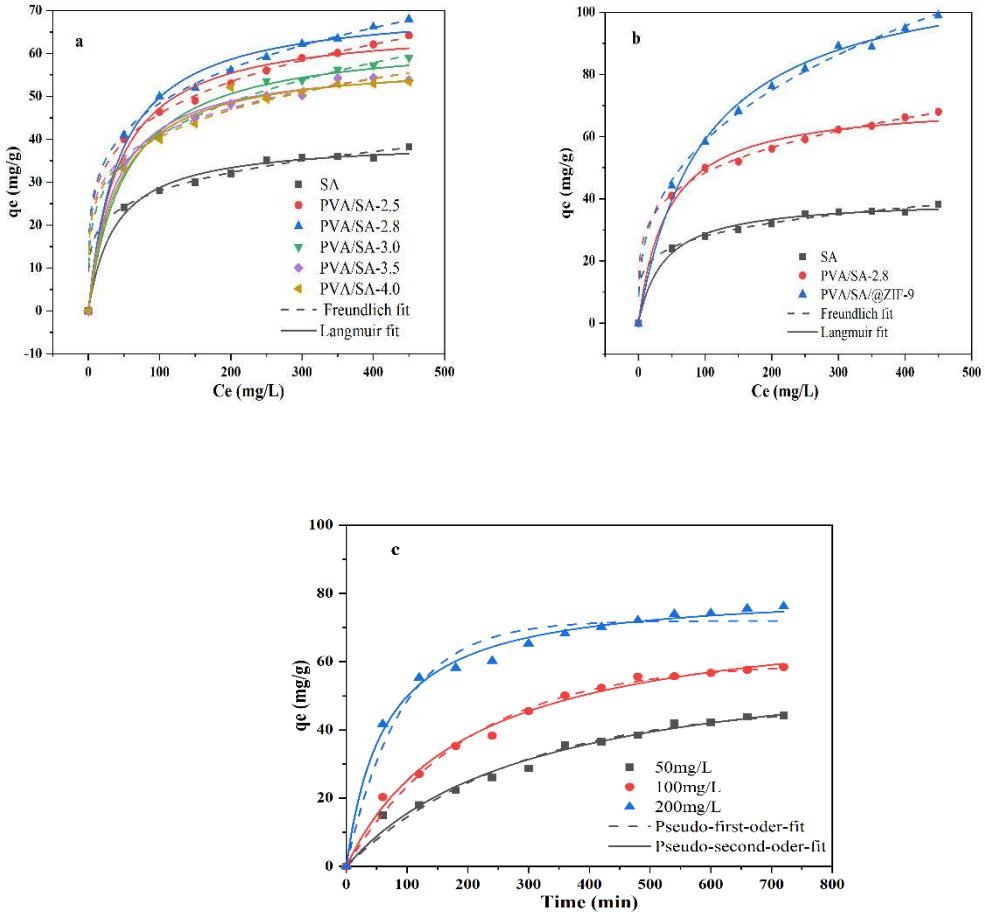

Fig. 8: (a) The adsorption isotherms of Cu(II) on SA, PVA/SA-2.5, PVA/SA-2.8, PVA/SA-3.0, PVA/SA-3.5, PVA/SA-4 hydrogels; (b) Adsorption isotherms of Cu(II)

on SA, PVA/SA-2.8 and PVA/SA@ZIF-9 hydrogels; (c) PVA/SA@ZIF-9-Cu hydrogels adsorption kinetic curves.

To study the interaction mechanism between hydrogels and Cu(II) and evaluate its adsorption capacity, two typical adsorption isotherm models, the Langmuir theoretical model and Freundlich theoretical are used to fit the experimental results, and their nonlinear forms are as follows:

$$q_e = \frac{K_L q_m c_e}{1 + K_L c_e} \quad (4)$$

$$q_e = K_F C_e^n \quad (5)$$

where, q_m is the theoretical maximum adsorption capacity of the adsorbent (mg/g); K_L is related to the adsorption energy Langmuir constant (L/mg); K_F represents the Freundlich constant [(mg/g)/(mg/L)$^{1/n}$] related to the adsorption capacity of the multilayer, n is a dimensionless parameter. Fig. 8(a) depicted the adsorption of Cu(II) on SA, PVA/SA-2.5, PVA/SA-2.8, PVA/SA-3.0, PVA/SA-3.5, PVA/SA-4 hydrogels adsorption isotherm at room temperature. As shown in the Figure, in the lower initial Cu(II) concentration range, the adsorption capacity of the adsorbent increases sharply. And with improving the initial concentration, the adsorption capacity increases slowly, the reason was the number of available active sites changed on the adsorbent surface. These results also suggest that with the increase of initial Cu(II) concentration, the total amount of adsorbed Cu(II) increases, and the adsorption capacity of PVA/SA@PAM-2.8 hydrogels was higher than that of SA, PVA/SA, and PVA/SA-3.0, PVA/SA-3.5, PVA/SA-4. The increase of SA content resulted in more hydroxyl (-OH) and carboxyl (-COOH) groups in the PVA/SA hydrogel. Therefore, a higher Cu(II) adsorption capacity can be obtained. However, the adsorption capacity decreased slightly with the further increase of SA concentration, which was caused by the reducing the chances of adsorbate capturing binding sites that was due to excessive crosslink density, similar to the work reported [33]. In addition, it can be seen from Fig. 8 (b) that the introduction of porous material ZIF-9 by in situ growth on PVA/SA-2.8 hydrogel improves the adsorption specific surface area of the

hydrogel material and enhances the adsorption performance of the composite material. Based on this, PVA/SA@ZIF-9 (SA content 2.8) was selected as the adsorbent for subsequent adsorption experiments.

Table 1 Adsorption isotherm parameters of different hydrogel materials for Cu(II)

Adsorbent	Langmuir isotherm				Freundlich isotherm		
	q_m (mg/g)	K_L (L/mg)	R_L	R^2	K_F (mg/g)	n	R^2
SA	39.79	0.025	0.0816-0.3798	0.933	10.934	0.2040	0.9714
PVA/SA-2.5	66.862	0.024	0.0844-0.3720	0.916	16.833	0.3626	0.9949
PVA/SA-2.8	71.31	0.023	0.0881-0.3620	0.934	17.280	0.3116	0.9925
PVA/SA-3.0	63.906	0.019	0.1047-0.3232	0.953	12.949	0.2632	0.9891
PVA/SA-3.5	57.99	0.026	0.0787-0.3884	0.959	16.506	0.2417	0.9753
PVA/SA-4.0	58.592	0.024	0.0851-0.3702	0.946	15.485	0.3094	0.9075
PVA/SA@ZIF-9	116.22	0.010	0.1818-0.2157	0.975	11.569	0.3524	0.9920

Tab. 1 shows the results and correlation coefficients obtained by fitting the Langmuir model and the Freundlich model to the experimental data. According to the correlation coefficient（R^2）, it can be seen that the adsorption data of SA, PVA/SA, and PVA/SA/@ZIF-9 show a better fit with the Freundlich model. In addition, the obtained constants R_L and n are between 0 and 1, which indicates that the adsorption reaction is easy to proceed with [34]. Besides, the Langmuir adsorption isotherm calculated that the maximum adsorption capacity of PVA/SA@ZIF-9

for Cu(II) was 116.22±3.73mg/g, and the experimental value was 98.98mg/g, which was about SA (39.79 ± 1.02mg/g).) and PVA/SA (71.31±2.01 mg/g) 2.9 times and 1.6 times. The results indicate that the composite porous material ZIF-9 has significantly enhanced the Cu(II) adsorption capacity of PVA/SA hydrogels.

Kinetic processes are also critical for evaluating potential adsorbent materials for practical applications. Fig. 9(c) depicts Cu(II) adsorption kinetics on PVA/SA@ZIF-9 gel spheres at different initial concentrations (50, 100, and 200 mg/L). In this experiment, pseudo-second-order and pseudo-first-order kinetic models are used to fit the experimental data, and their nonlinear forms are as follows:

$$q_t = q_e(1 - e^{K_1 t}) \quad (6)$$

$$q_t = \frac{k_2 q_e^2 t}{1 + k_2 q_{et}} \quad (7)$$

where, K_1 (1/min) and K_2 [g/(mg • min)] and t (min) are the rate constants associated with the pseudo-first-order kinetic model, the rate constant and time of the pseudo-second-order kinetic model, respectively.

Table 2 Adsorption kinetic parameters of PVA/SA@ZIF-9 for different initial Cu(II) concentrations

		Pseudo first-order model			Pseudo second-order model		
C_0 (mg/L)	$q_{e,exp}$ (mg/g)	$q_{e,cal}$ (mg/mg)	k_1 (1/min)	R^2	$q_{e,cal}$ (mg/mg)	k_1 [g/(mg ·min)]	R^2
50	44.2	47.5±2.2	0.0036	0.9757	63.9±3.9	0.00005	0.9811
100	58.4	59.7±1.2	0.0004	0.9816	76.1±2.3	0.00006	0.9920
200	76.2	71.9±1.5	0.0119	0.9625	81.2±1.3	0.00019	0.9915

The influence of contact time on the adsorption efficiency of Cu(II) was

discussed (Fig. 8c). The adsorption capacity of PVA/SA@ZIF-9-Cu increased rapidly from 41.76 mg/g to 68.2 mg/g as the time increased from 1h to 6h at the initial concentration was 200mg/L. Then, the increased rate of adsorption capacity decreased with the extension of adsorption time, which indicated that the adsorption active sites were gradually depleted, and the adsorption reached saturation. The rapid absorption rate in the initial phase was due to sufficient unoccupied adsorption sites and a large concentration gradient as the driving force;

the Cu (II) in the solution slowly penet rated the PVA/SA@ZIF-9 composite hydrogels and occupied th e internal active sites. After the active areas were gradually saturated, resulting in a decrease in the adsorption rate of Cu(II) until equilibrium is reached [30]. Based on the results above, a reaction time of 12 h was used as the reaction condition for the subsequent adsorption experiments.

Table 2 presents the results of relevant experimental data by pseudo-first-order and pseudo-second-order kinetic models. It is showed that the linear correlation coefficient of the pseudo-second-order kinetic model (R^2=0.981, 0.992, and 0.991) was better than that of the pseudo-first-order kinetic model (R^2=0.975, 0.981 and 0.962) at different initial concentrations (50, 100, and 200 mg/L) Therefore, the adsorption process of Cu(II) on PVA/SA@ZIF-9 composite hydrogels was chemical adsorption[35].

4.2.3 The effect of temperature and adsorption thermodynamics

Thermodynamic studies were carried out at 293.15、298.15、303.15、308.15 、 313.15K temperature, respectively. The results were shown in Fig. 9(a). With the increase in temperature, the adsorption of Cu(II) by PVA/SA increased. The

the adsorption process is endothermic.

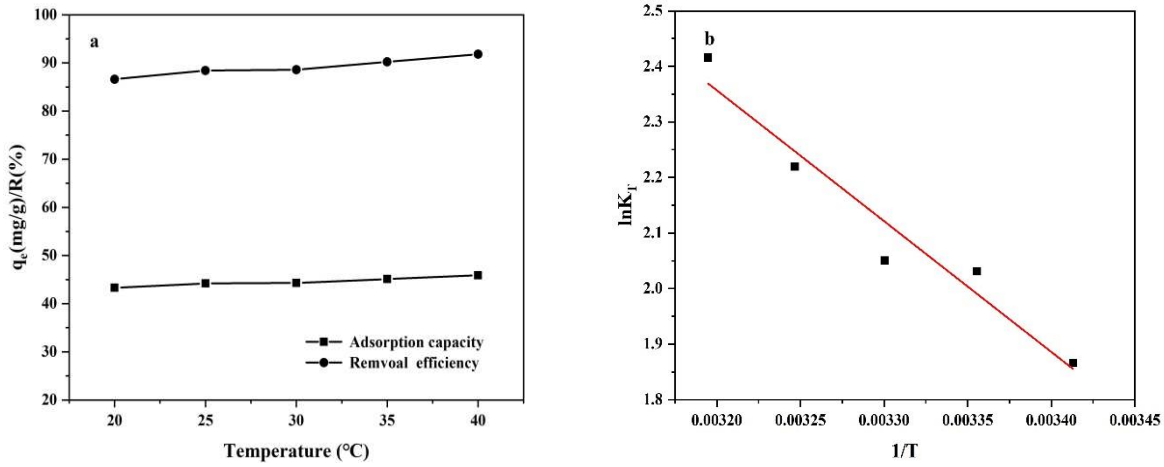

Fig. 9: (a) Effect of temperature on the adsorption of Cu(II) on PVA/SA@ZIF-9 (b) van'tHoff's curves

The thermodynamic parameters such as enthalpy change $\triangle H^0$(KJ/mol), entropy Change $\triangle S^0$ [J/(mol•K)], and Gibbs free energy $\triangle G^0$ (KJ/mol) in the adsorption the process is calculated by the following formula：

$$\ln K_T = \frac{\Delta S^0}{R} - \frac{\Delta H^0}{RT} \quad (8)$$

$$\Delta G^0 = -RT \ln K_T \quad (9)$$

$$K_T = \frac{q_e}{C_e} \quad (10)$$

where, q_e and C_e are the equilibrium adsorption capacity and equilibrium concentration respectively at the corresponding temperature, K_T (L/g), R (8.314kJ/mol), and T (K) are represented as the equilibrium constant, the universal gas constant, and absolute temperature, respectively. Fig. 9(b) was the van'tHoff's curve of the corresponding temperature.

Table 3 Thermodynamic parameters of Cu(II) adsorption by PVA/SA@ZIF-9

Temperature(K)	$\ln K_T$	$\triangle G^0$(KJ/mol)	$\triangle H^0$(KJ/mol)	$\triangle S^0$[J/(mol•K)]
293	1.87	-4.55		
298	2.03	-5.03		
303	2.05	-5.17	19.5814	82.2562
308	2.22	-5.68		
313	2.42	-6.29		

The thermodynamic parameters are shown in Table 3. It can be observed from the table that $\triangle G^0$ was negative at a different temperature, indicating that the adsorption process was spontaneous and it was beneficial to the adsorption process at a higher temperature. In addition, the positive value of the parameter $\triangle H^0$=19.5814 obtained by curve fitting also indicates that the adsorption was an endothermic process. A positive value of $\triangle S^0$ suggests that PVA/SA has a higher affinity for Cu(II).

4.2.4 Recycling performance evaluation experiment

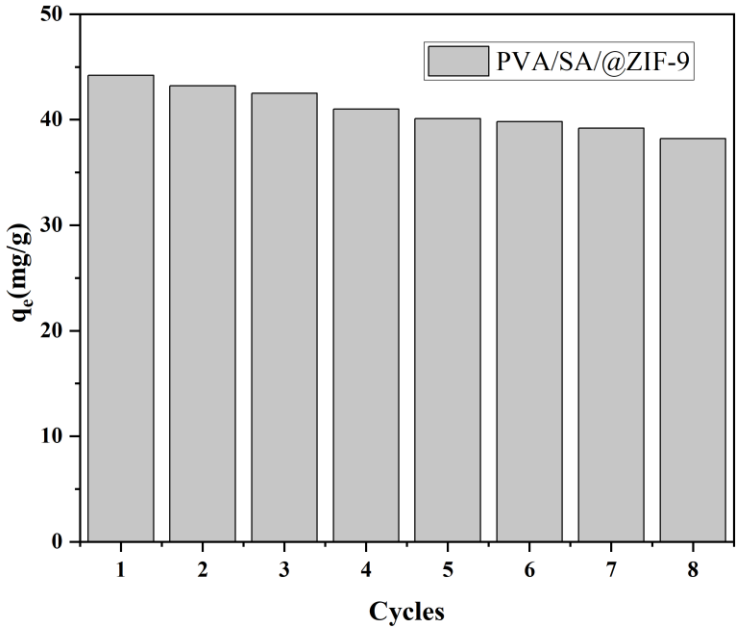

Fig.10 Recycling performance of PVA/SA@ZIF-9 hydrogels (Dose=1g/L, pH=5, C_0=50mg/L, t=24h, T=25℃)

The recycling performance of PVA/SA@ZIF-9 hydrogels is shown in Fig. 10, and the experimental results suggest that the adsorption capacity Cu(II) of the PVA/SA@ZIF-9 hydrogels decreased slightly with using dilute acid as the eluent to regenerate the adsorbent after several cycles of adsorption and desorption experiments. The adsorption capacity from the first to the eighth time was 44.2 mg/g to 38.2 mg/g, which maintained an excellent removal effect. The structure of the hydrogels remained intact and presented no apparent difference.

5 Conclusion

The PVA/SA composite hydrogel material prepared by in situ growth composite ZIF-9 significantly enhanced the adsorption effect of sodium alginate hydrogel on Cu(Ⅱ). The experimental results show that complexation, cation exchange, and physical adsorption are the main adsorption mechanisms, and -OH and -COOH in the composite material are involved in the adsorption process and the result of ion exchange between Ca^{2+} and Cu^{2+}. PVA/SA@ZIF-9 shows the maximum adsorption capacity for Cu(II) (98.98 mg/g) under optimal conditions, approximately 2.6 and 1.5 times that of ordinary SA and PVA/SA hydrogels. The adsorption-desorption cycle performance research experiments further demonstrated the excellent adaptability and mechanical stability of PVA/SA@ZIF-9. Therefore, considering the simple production process, low cost of raw materials, good adsorption capacity, strong adaptability, and good mechanical stability, the synthesized PVA/SA@ZIF-9 is feasible for some experimental heavy metal-

containing wastewater treatment.

CRediT authorship contribution statement

Guojun Zhang: Experimentalize, Data collection, Writing-original draft. Guijun Yang: Investigation, Aid with Synthesis and Preliminary Characterization. Huiyuan Chen: Data curation, Formal analysis. Hua Fu: Supervision, Writing-review & editing.

Declaration of competing interest

The authors declare that they have no known competing financial interests or personal relationships that could have appeared to influence the work reported in this paper.

Acknowledgements

The authors are grateful for the financial support from Qinghai Province Thousand Talents Program funded project.

References

[1]Liu T, Chen Z, Li Z, et al. Rapid Separation and Efficient Removal of Cd Based on Enhancing Surface Precipitation by Carbonate-Modified Biochar. ACS omega 28 (6) (2021): 18253-18259. https://doi.org/10.1021/acsomega.1c02126.

[2]Liu C , Wu T , Hsu P C , et al. Direct/Alternating Current Electrochemical Method for Removing and Recovering Heavy Metal from Water Using Graphene Oxide Electrode. 13(6) (2019) 6431-6437. https://doi.org/10.1021/acsnano.8b09301.

[3]Yang L , Zhu Y J , He G , et al. Multifunctional Photocatalytic Filter Paper Based on Ultralong Nanowires of the Calcium-Alendronate Complex for High-Performance Water Purification. 14 (7) (2022) 9464-9479. https://doi.org/10.1021/acsami.1c23180.

[4]Khan, M. , Akhtar, A. , & Nabi, S. A. Kinetics and thermodynamics of alkaline earth and heavy metal ion exchange under particle diffusion controlled phenomenon using polyaniline-sn(iv)iodophosphate nanocomposite. Journal of Chemical & Engineering Data, 59(8)(2014), 2677-2685.https://doi.org/10.1021/je500523n.

[5] Mfm A , Amgm B , Mk C , et al. Adsorption of heavy metals and hardness ions from groundwater onto modified zeolite: Batch and column studies. Alexandria Engineering Journal, 2022. https://doi.org/10.1016/j.aej.2021.09.041.

[6] Es-Sahbany H , Hsissou R , Hachimi M , et al. Investigation of the adsorption of heavy metals (Cu, Co, Ni and Pb) in treatment synthetic wastewater using natural clay

as a potential adsorbent (Sale-Morocco). Materials Today: Proceedings, 2021. https://doi.org/10.1016/j.matpr.2020.12.1100.
[7] Liu S , Zhang S , Fan M , et al. High-efficiency adsorption of various heavy metals by tea residue biochar loaded with nanoscale zero-valent iron. Environmental Progress & Sustainable Energy, 2021. https://doi.org/10.1002/ep.13706.
[8]Jatinder Kaur, Parbati Sengupta, and Samrat Mukhopadhyay.Critical Review of Bioadsorption on Modified Cellulose and Removal of Divalent Heavy Metals (Cd, Pb, and Cu). Industrial & Engineering Chemistry Research. 61 (5)(2022)1921-1954. https://doi.org/10.1021/acs.iecr.1c04583.
[9] Zuo Q , Zheng H , Zhang P , et al. Functionalized Activated Carbon Fibers by Hydrogen Peroxide and Polydopamine for Efficient Trace Lead Removal from Drinking Water.Langmuir . 38 (1) (2022) 253–263. https://doi.org/10.1021/acs.langmuir.1c02459.
[10] Zhao Z , Song Y , Phanlavong P , et al. Efficient Heavy Metal Removal from Water by Polydopamine Confined ZrO_2 Nanocrystals with Improvements in Nanoparticles Utilization and Ion Diffusion. (2022). https://doi.org/10.1021/acsestengg.1c00370.
[10] Zhao Z , Song Y , Phanlavong P , et al. Efficient Heavy Metal Removal from Water by Polydopamine Confined ZrO_2 Nanocrystals with Improvements in Nanoparticles Utilization and Ion Diffusion. (2022). https://doi.org/10.1021/acsestengg.1c00370.

[11] Xue S , Fan J , Wan K , et al. Calcium-Modified Fe3O4 Nanoparticles Encapsulated in Humic Acid for the Efficient Removal of Heavy Metals from Wastewater. Langmuir. 37(2021), 10994-11007. https://doi.org/10.1021/acs.langmuir.1c01491.
[12] Jayaramudu T , Pyarasani R D , Akbari-Fakhrabadi A , et al. Synthesis of Gum Acacia Capped Polyaniline-Based Nanocomposite Hydrogel for the Removal of Methylene Blue Dye. Journal of Polymers and the Environment. 29(2021) 2447–2462, https://doi.org/10.1007/s10924-021-02066-w.
[13] Yan Y Z, An Q D, Xiao Z Y, et al. Flexible core-shell/bead-like alginate@PEI with exceptional adsorption capacity, recycling performance toward batch and column sorption of Cr(VI). Chemical Engineering Journal, 313 (2017) 475-486,

https://doi.org/10.1016/j.cej.2016.12.099.

[14] Choi，H.J. Assessment of the adsorption kinetics，equilibrium and thermodynamic for Pb(II) removal using alow-costhybrid biowaste adsorbent eggshell/coffeeground/sericite. Water Environ.Res. 91 (12) (2019) 1600-612, https://doi.org/10.1002/wer.1158.

[15] Zhang W , Song J , He Q , et al. Novel pectin based composite hydrogel derived from grapefruit peel for enhanced Cu(II) removal. Journal of Hazardous Materials, 384(2019) 121445, https://doi.org/10.1016/j.jhazmat.2019.121445.

[16] Huixue, Ren, Zhimin, et al. Efficient Pb(II) removal using sodium alginate-carboxymethyl cellulose gel beads: Preparation, characterization, and adsorption mechanis, Carbohydrate polymers, (2016), https://doi.org/10.1016/j.carbpol.2015.11.002.

[17] Yuan L , Wu Y , Gu Q S , et al. Injectable photo crosslinked enhanced double-network hydrogels from modified sodium alginate and gelatin. International Journal of Biological Macromolecules, 96 (2017) 569-577. https://doi.org/10.1016/j.ijbiomac.2016.12.058.

[18] Li Y , Liu S J , Chen F M , et al. High-Strength Apatite/Attapulgite/Alginate Composite Hydrogel for Effective Adsorption of Methylene Blue from Aqueous Solution. Journal of Chemical & Engineering Data, 64(12)(2019), https://doi.org/10.1021/acs.jced.9b00616.

[19] Cheng P , Wang C , Kaneti Y V , et al. Practical MOF Nanoarchitectonics: New Strategies for Enhancing the Processability of MOFs for Practical Applications. Langmuir, 36(16)(2020), https://doi.org/10.1021/acs.langmuir.0c00236.

[20] Lohe M R , Rose M , Kaskel S . Metal-organic framework (MOF) aerogels with high micro-and macroporosity. Chemical Communications, 40 (2009) 6056-6058, https://doi.org/10.1039/b910175f.

[21] Eltaweil A S, Mamdouh I M, Abd El-Monaem E M, et al. Highly efficient removal for methylene blue and Cu^{2+} onto UiO-66 metal-organic framework/carboxylated graphene oxide-incorporated sodium alginate beads. ACS omega, 6(36) (2021) 23528-23541, https://doi.org/10.1021/acsomega.1c03479.

[22] Cao J, Su Y, Liu Y, et al. Self-assembled MOF membranes with underwater superoleophobicity for oil/water separation. Journal of Membrane Science, 566 (2018) 268-277, https://doi.org/10.1016/j.memsci.2018.08.068.

[23] He Zhu, Qi Zhang, Shiping Zhu.Alginate Hydrogel: A Shapeable and Versatile Platformfor In-Situ Preparation of MOF-Polymer Composites.ACS Applied Materials & Interfaces.2016, 8, 17395−17401.

[23] Peixia, Zhao, et al. In-situ growth of polyvinylpyrrolidone modified Zr-MOFs thin-film nanocomposite (TFN) for efficient dyes removal. Composites Part B Engineering, (2019), https://doi.org/10.1016/j.compositesb.2019.107208.

[24] Maan O , Song P , Chen N , et al. An In Situ Procedure for the Preparation of Zeolitic Imidazolate Framework-8 Polyacrylamide Hydrogel for Adsorption of Aqueous Pollutants. Advanced Materials Interfaces, (2019). https://doi.org/10.1002/admi.201801895.

[25] Zhu H , Zhang Q , Zhu S . Alginate Hydrogel: A Shapeable and Versatile Platform for in Situ Preparation of Metal-Organic Framework-Polymer Composites. Acs Appl Mater Interfaces, (2016)17395, https://doi.org/10.1021/acsami.6b04505.

[26] Ren W , Gao J , Lei C , et al. Recyclable metal-organic framework/cellulose aerogels for activating peroxymonosulfate to degrade organic pollutants. CHEMICAL ENGINEERING JOURNAL -LAUSANNE-, (2018), https://doi.org/10.1016/j.cej.2018.05.143.

[24] Qian D , Bai L , Wang Y , et al. A Bifunctional Alginate-Based Composite Hydrogel with Synergistic Pollutant Adsorption and Photocatalytic Degradation Performance. Industrial&Engineering Chemistry Research, 58 (29) (2019). https://doi.org/10.1021/acs.iecr.9b01709.

[25] Kwon O H , Kim J O , Cho D W , et al. Adsorption of As(III), As(V) and Cu(II) on zirconium oxide immobilized alginate beads in aqueous phase[J]. Chemosphere, 160 (oct) (2016) 126-133, https://doi.org/10.1016/j.chemosphere.2016.06.074..

[26] Hu T , Liu Q , Gao T , et al. Facile Preparation of Tannic Acid‐Poly(vinyl alcohol)/Sodium Alginate Hydrogel Beads for Methylene Blue Removal from Simulated Solution. ACS Omega, 3 (7) (2018) 7523-7531, https://doi.org/10.1021/acsomega.8b00577.

[27] Morsy M A , Al-Khaldi M A , Suwaiyan A . Normal Vibrational Mode Analysis and Assignment of Benzimidazole by ab Initio and Density Functional Calculations and Polarized Infrared and Raman Spectroscopy. The Journal of Physical Chemistry A, 106 (40) (2002) 9196 – 9203, https://doi.org/10.1021/jp0256948.

[28] Zhang X , Lin X , He Y , et al. Phenolic hydroxyl derived copper alginate microspheres as superior adsorbent for effective adsorption of tetracycline. International Journal of Biological Macromolecules, 136 (2019), https://doi.org/10.1016/j.ijbiomac.2019.05.165.

[29] Zhu X , Liu Y , Zhou C , et al. A novel porous carbon derived from hydrothermal carbon for efficient adsorption of tetracycline. Carbon, 77(2014) 627-636, https://doi.org/10.1016/j.carbon.2014.05.067.

[30] Xu X , Jiang X Y , Jiao F P , et al. Tunable assembly of porous three-dimensional graphene oxide-corn zein composites with strong mechanical properties for adsorption of rare earth elements. Journal of the Taiwan Institute of Chemical Engineers, (2018):S187610701730665X. https://doi.org/10.1016/j.jtice.2017.12.024.

[31] Jin, Can, Zhang, et al. Thiol-Ene Synthesis of Cysteine-Functionalized Lignin for the Enhanced Adsorption of Cu(II) and Pb(II). Industrial & Engineering Chemistry Research, 57 23 (2018) 7872–7880, https://doi.org/10.1021/acs.iecr.8b00823.

[32] Chen X , Chen G , Chen L , et al. Adsorption of copper and zinc by biochars produced from pyrolysis of hardwood and corn straw in aqueous solution. Bioresource Technology, 102 (19) (2011) 8877-8884, https://doi.org/10.1016/j.biortech.2011.06.078.

[33] Periyasamy S , N Viswanathan. Hydrothermal Synthesis of Melamine-Functionalized Covalent Organic Polymer-Blended Alginate Beads for Iron Removal from Water[J]. Journal of Chemical & Engineering Data, (2019) , https://doi.org/10.1021/acs.jced.8b01085.

[34] Wang N , Xu X , Li H , et al. Preparation and Application of a Xanthate-Modified Thiourea Chitosan Sponge for the Removal of Pb(II) from Aqueous Solutions. Industrial & Engineering Chemistry Research, 55 (17) (2016) 4960-4968, https://doi.org/10.1021/acs.iecr.6b00694.

[35] Nguyen T A , Dang B T , Le H , et al. Thiosemicarbazone-Modified Cellulose: Synthesis, Characterization, and Adsorption Studies on Cu(II) Removal. ACS Omega, 5 (24) (2020) 14481-14493, https://doi.org/10.1021/acsomega.0c01129.